City Research Online

City, University of London Institutional Repository

This is the unspecified version of the paper.

This version of the publication may differ from the final published version.

Design of bent photonic crystal fiber supporting a single polarization

B. M. Azizur Rahman,* Muhammad Uthman, Namassivayane Kejalakshmy,
Arti Agrawal, and Kenneth T. V. Grattan

City University London, School of Engineering and Mathematical Sciences, Northampton Square, London EC1V 0HB, UK

*Corresponding author: B.M.A.Rahman@city.ac.uk

In this work, it is shown that the differential loss between the TE- and TM-polarized fundamental modes in a highly birefringent photonic crystal fiber (PCF) can be enhanced by bending the fiber. As a result, a design approach for single-mode single-polarization operation has been developed and is discussed. A rigorous full-vectorial **H**-field-based finite element approach, which includes the conformal transformation and the perfectly matched layer, is used to determine the single-polarization properties of such a highly birefringent PCF by exploiting its differential bending losses.   © 2011 Optical Society of America

OCIS codes: 060.5295, 260.1440.

1. Introduction

Photonic crystal fibers (PCFs) [1] can be widely used as waveguides or photonic devices allowing the exploitation of their single-mode property, higher modal birefringence, adjustable spot size, and tailorable dispersion properties for various linear and nonlinear applications. Initially, PCF was considered to be an endlessly single-mode fiber, but later numerical studies, such as through the multipole method and finite element method (FEM), have revealed that the cutoff conditions are critically controlled by the diameter-to-pitch ratio [2–4]. Ordinary PCF, with its 60° rotational symmetry, is only weakly birefringent. However, by assigning unequal diameter-to-pitch ratios, it is possible to invoke the birefringence between the otherwise nearly degenerate TE and TM modes and PCFs of this type can maintain the polarization state of the optical signal. The properties of the TE and TM modes can be further tuned to have different cutoff conditions by adjusting the diameters of the air-hole-to-pitch ratio. These concepts can be exploited to design effective single-mode single-polarization (SMSP) fibers. However, the novelty of

this work is that the differential loss ratio (LR) between the polarized modes can be further enhanced and controlled by adjusting the bending radius of these highly birefringent PCFs, this being shown here for the first time to our knowledge. Thus, in this work, the SMSP properties of highly birefringent PCFs have been analyzed by using a rigorous full-vectorial **H**-field-based FEM.

A. FEM Modal Solution for PCF

In the modal solution approach based on the FEM, the intricate cross section of a PCF can be represented by using many triangles of different shapes and sizes. This flexibility makes the FEM preferable as a technique to use when compared to the finite difference method, which not only uses inefficient regular spaced meshing, but also cannot represent the slanted or curved dielectric interfaces. The optical modes in a high index contrast PCF with two-dimensional confinement are also hybrid in nature, with all six components of the **E** and **H** fields being present. It is also known that the modal hybridness is enhanced by the presence of slanted or curved dielectric interfaces. Hence, not only is a vectorial formulation needed for the accurate determination of their modal solutions but also a proper representation of the dielectric interfaces is important. In the

present approach, an **H**-field-based rigorous full-vectorial FEM has been used to analyze the SMSP operation regime of PCFs with air holes arranged in a triangular lattice in the silica cladding. The **H**-field formulation developed previously [5] is a valid approach for microwave and optical guided-wave devices, including the intermediate terahertz frequency range. The **H**-field formulation with the augmented penalty function technique is given below:

$$\omega^2 = \frac{\left(\int(\nabla \times \vec{\mathbf{H}}) * \cdot \hat{\varepsilon}^{-1}(\nabla \times \vec{\mathbf{H}})\mathrm{d}\Omega\right) + \left(\int(\alpha/\varepsilon_o)(\nabla \cdot \vec{\mathbf{H}}) * (\nabla \cdot \vec{\mathbf{H}})\mathrm{d}\Omega\right)}{\int \vec{\mathbf{H}} * \cdot \hat{\mu}\vec{\mathbf{H}}\mathrm{d}\Omega}, \tag{1}$$

where $\vec{\mathbf{H}}$ is the full-vectorial complex magnetic field, $\hat{\varepsilon}$ and $\hat{\mu}$ are the permittivity and permeability, respectively, of the waveguide, ε_0 is the permittivity of the free space, ω^2 is the eigenvalue (where ω is the angular frequency of the wave), and α is a dimensionless parameter used to impose the divergence-free condition of the magnetic field in a least squares sense. In this formulation, both the $\hat{\varepsilon}$ and $\hat{\mu}$ parameters can be arbitrary complex tensors with possible off-diagonal coefficients, suitable to characterize electro-optic, acousto-optic, and elasto-optic devices. To calculate the leakage and bending losses, perfectly matched layers (PMLs) [6] have been incorporated around the computation window, and this makes the resulting formulation a complex eigenvalue equation. The PML parameters for the parabolic conductivity profile were optimized to achieve high numerical stability. For a straight waveguide, a twofold symmetry is available; however, for a bent PCF, only half of the PCF structure has been considered due to the existing onefold symmetry. In this paper, the characterization of the SMSP of a PCF with a solid silica core has been analyzed using the full-vectorial FEM.

2. Results

A. Straight SMSP PCF

In this study, index guiding silica PCF with the air holes arranged in a triangular lattice is considered first, with the diameter of an air hole denoted by d and the distance (pitch) between two air holes by Λ. A missing air hole constitutes the effective core of the PCF. The refractive index of the silica used is taken as 1.444 at an operating wavelength of $1.55\,\mu\mathrm{m}$. A typical PCF with 60° rotational symmetry can support two fundamental H_{11}^y (quasi-TE) and H_{11}^x (quasi-TM) modes and higher Λ and d/Λ values, but it may also support additional higher-order modes of a given polarization. This structure possesses weak birefringence as it does not have the necessary 90° rotational symmetry, which has often

been ignored. The modal birefringence of a PCF can be increased by breaking the natural symmetry of having sized air holes of identical diameters. Initially, the asymmetric arrangement considered here is similar to that considered in previous work [4,7], where the diameters (d_2) of the four air holes in the first ring are larger than those of the other air-hole diameters (d). Later on, orientation of the structural asymmetry is also studied for a bent PCF. In Fig. 1, the variations of the effective indices of the quasi-TE and quasi-TM modes, with respect to the ratio d_2/Λ, are shown for a PCF with $d/\Lambda = 0.5$ and $\Lambda = 1.6\,\mu\mathrm{m}$. For this arrangement, as its equivalent height is smaller than its equivalent width, the effective index of the quasi-TM (H_{11}^x) mode is lower than that of the quasi-TE (H_{11}^y) mode. This also yields a significantly high modal birefringence. Here, the birefringence is defined as the difference between the effective indices of the H_{11}^y and H_{11}^x modes. The quasi-TM mode (with the dominant H^y and E^x fields) has a smaller effective index value, is slightly weakly confined compared to the TE mode, and expands more into the cladding region, which also makes it highly exposed to the bigger air holes. It can be observed that, as the value of d_2/Λ increases, the structural asymmetry increases further, as does the modal birefringence. It should be noted that the modal birefringence shown here is higher than that of a "panda" or "bow-tie" fiber and this can be achieved by using simple air-hole diameter adjustment.

Since all the PCF designs considered have a higher index solid silica region beyond the air-hole rings, all the modes suffer from leakage losses, which are critically dependent on their structural parameters. The PMLs are used around the orthodox
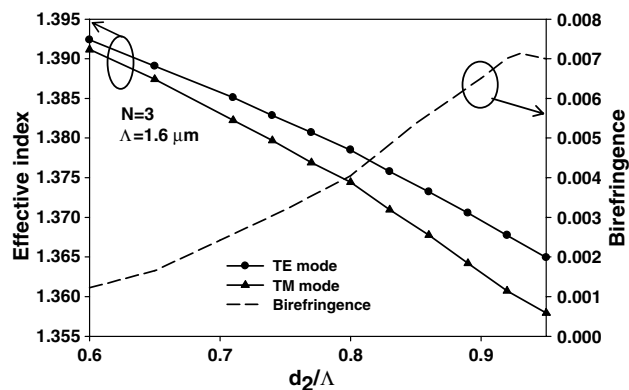

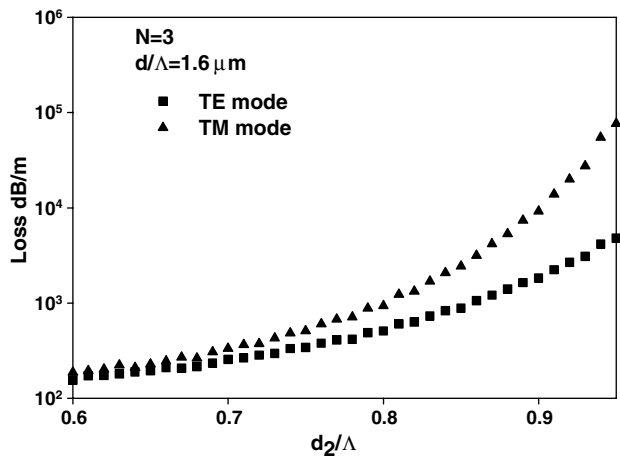Fig. 1. Variation of effective index and birefringence with the d_2/Λ.

Fig. 2. Variations of the TE and TM modal losses with the d_2/Λ.

Fig. 3. (Color online) Variation of the differential LR with d_2/Λ for pitches 1.6 and 1.8 μm.

computational window to calculate the leakage and bending losses. The variations of the modal losses for the quasi-TE and quasi-TM modes with the d_2/Λ value are shown in Fig. 2. As d_2 increases, the overall dimension of the core reduces for both the polarized modes and, along with this, by choosing a lower Λ, a PCF can be designed so that it approaches selectively the cutoff conditions of two polarized modes. It can be observed that, as the ratio d_2/Λ is increased, both the polarized fundamental modes approach their cutoff conditions and their leakage loss values also increase. However, Fig. 2 shows that the loss of the TM mode is higher than that of the TE mode and, further, it can be seen that the difference between their values is increasing with the d_2/Λ value. As the effective index of the TM mode is lower, it approaches its cutoff condition at a lower value of d_2/Λ and this mode suffers a higher loss compared to that of the TE mode. This differential loss allows for the possibility of designing a feasible SMSP PCF.

To develop the design of a SMSP PCF, the characteristics of a dimensionless differential LR are studied. This parameter, LR, can be defined as the ratio of leakage loss of the TM mode (α_{TM}) to the leakage loss of the TE mode (α_{TE}), as follows:

$$\text{LR} = \frac{\alpha_{TM}}{\alpha_{TE}}. \qquad (2)$$

The variations of the differential loss values for two different pitch lengths, Λ, are shown in Fig. 3. This shows that, as the value of d_2/Λ is increased, the differential LR also increases. This can allow the TM modes to be suppressed effectively when compared to the guidance of TE mode with a relatively smaller loss. By reducing the pitch length, Λ, a PCF can be operated closer to the cutoff condition and the loss for both the polarized modes will be increased, but this also increases the differential LR, as is shown in this figure. It can be noted that LR increases exponentially when the H_{11}^x mode reaches its cutoff, but, in this case, the loss for the H_{11}^y can
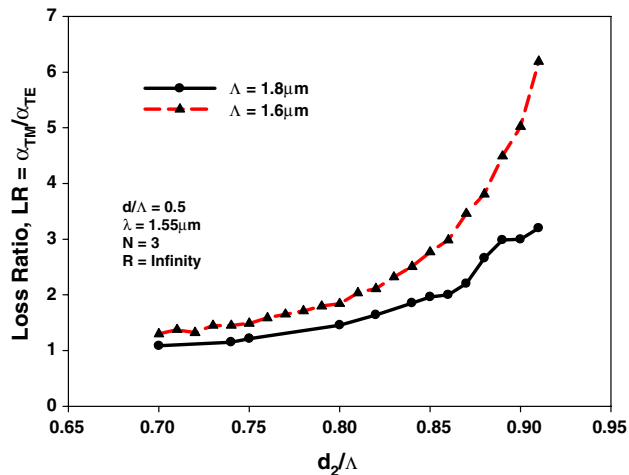
also be high. Some deviations from the trend of their curves can be observed that are due to the degeneration of the core mode with the surface modes (in the silica bridges or cladding region) and similar features were reported earlier [8]. By optimizing the PCF parameters, such as the pitch length, Λ, the d_2/Λ ratio, and the number of rings, it would appear possible to achieve suitable SMSP operation of a PCF [4].

B. Bent SMSP PCF

It is also known that a bent PCF suffers from an additional bending loss, and the bending can also influence the cutoff condition of a PCF. This can be exploited further in the optimization of the design. In this subsection, a novel approach is reported where the effect of bending to enhance the SMSP operation of a PCF is considered for the first time. To study the effects of arbitrary bends, various numerical methods have been developed and used to simulate the light propagation in bent waveguides with the aim of characterizing the bending, the transition, and the polarization losses. The conformal transformation [9] has been most widely used to represent such bent waveguides by converting a curved dielectric waveguide to its equivalent straight waveguide with a modified index profile. The coordinate transformation allows a bent optical waveguide in the x plane to be represented by an equivalent straight waveguide with a modified refractive index distribution, $n_{eq}(x,y)$ [9]:

$$n_{eq}(x,y) = n(x,y)\left(1 + \frac{x}{R}\right), \qquad (3)$$

where $n(x,y)$ is the original refractive index profile of the bent waveguide, $n_{eq}(x,y)$ is the equivalent index profile of a straight guide, R is the radius of curvature, and x is the distance from the center of the waveguide. With a reduction in the bending radius, the cladding in the outer side (away from bending center) encounters a higher equivalent index
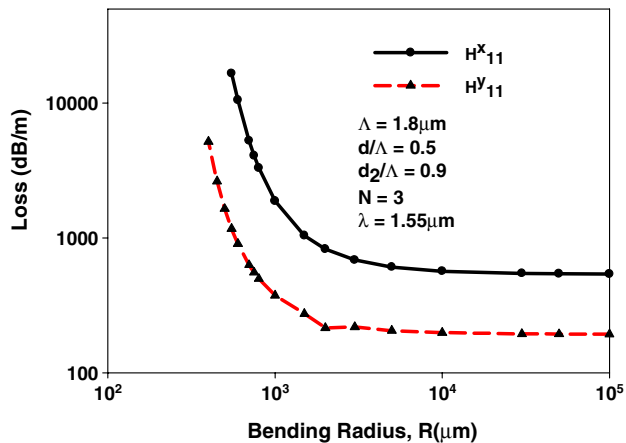
Fig. 4. (Color online) TE and TM modal losses with the bending radius, R, for $\Lambda = 1.8\,\mu$m.

Fig. 5. (Color online) Variation of the bending losses with the bending radius, R, of the TM modes for different d_2/Λ ratios.

compared to the inner side cladding and, hence, the fundamental mode shifts farther outward, with a slight increase in the modal effective index value. The shift of the modal field toward the raised equivalent cladding index increases the leakage loss due to this bending, which increases further for a lower bending radius.

The variation of the bending losses for the quasi-TE and quasi-TM modes with the bending radius are shown in Fig. 4 for a highly birefringent PCF. This shows that both the TE and TM modal losses increase with the reduced bending radius, R. It should be noted that, with H_{11}^x being closer to the cutoff, the leakage loss is higher than that of the H_{11}^y mode and, additionally, the bending loss increases more rapidly with the bending and reaches its cutoff condition sooner. When a PCF is bent, its mode field also shifts away from the center of the waveguide. Our numerical simulation indicates that butt-coupling loss between a straight PCF and a bent PCF with $R = 0.7$ cm (both with $\Lambda = 1.8\,\mu$m, $d/\Lambda = 0.5$, $d_2/\Lambda = 0.9$, $\lambda = 1.55\,\mu$m) would be less than 0.4 dB.

The bending loss also depends strongly on the air-hole diameter, as its combination with the pitch value (Λ) can dictate the cutoff conditions. It is known that larger air-hole diameters (d_2) reduce the core size and, as a result, the cutoff conditions occur more rapidly. The variations of the bending losses with the bending radius, R, for different d_2/Λ values for the quasi-TM (H_{11}^x) modes are shown in Fig. 5. This shows that the bending loss of the H_{11}^x mode for different air-filling fractions can also be controlled by the diameter of the four larger air holes (d_2) in the first ring. It can be noted that, for higher d_2/Λ ratios, the initial leakage loss is higher (when $R = \infty$), and also that it reaches its cutoff condition sooner, as the bending radius is reduced. However, it can be noted that the maximum loss values are very similar for all the d_2/Λ values. The variation of the bending loss with the bending radius for the quasi-TE (H_{11}^y) mode also shows a similar trend but with a lower value (not shown here) and cutoff can be reached, but it requires a smaller value of R.
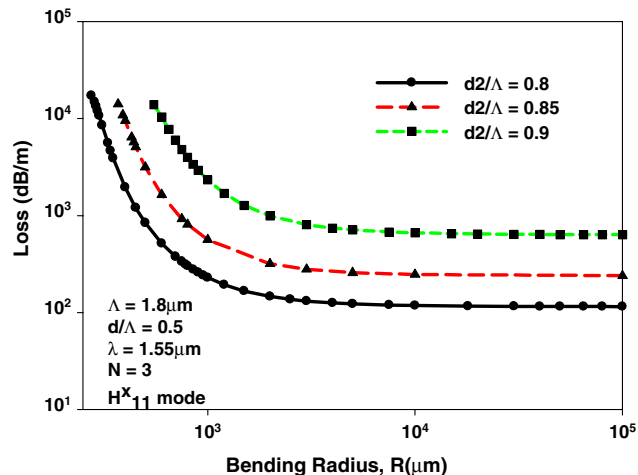
To quantify the single-polarization properties, the variations of the loss ratio (LR) values with the bending radius are shown in Fig. 6 for different d_2/Λ values. It can be observed that the differential loss ratio (LR) is higher for a more asymmetric PCF, when the d_2/Λ value is higher. In all cases, it is also shown here that the differential loss can be substantially increased by reducing the bending radius. It can be seen that there is a critical value of the bending radius, R_c, below which LR increases rapidly with any further reduction of the bending radius. In Fig. 3, it was shown that the differential LR can be controlled by adjusting the structural asymmetry, via its d_2/Λ value. However, once a PCF is fabricated according to a given design specification, the actual LR value can be slightly different due to the fabrication errors. On the other hand, in Fig. 6, it is shown that the LR value can also be continuously controlled via adjusting the bending radius for a given structural asymmetry. Since the bending radius can always be adjusted, this would allow for the compensation of any possible fabrication errors.
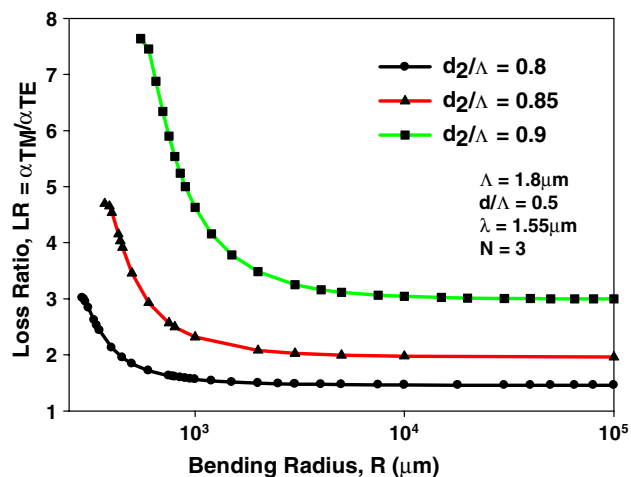

Fig. 6. (Color online) Variation of LR with the bending radius for different d_2/Λ values.

C. Effect of Number of Rings on the Bent SMSP PCF

It is also known that both the leakage loss and the bending loss can be controlled by increasing the number of air-hole rings. However, here the objective is to study the enhancement of the differential loss but with a reasonably lower loss value for the H_{11}^y mode, by adjusting the number of air-hole rings (N). As N increases, both the TE and TM modes become well confined. However, with bending, the tightly confined modes tend to move toward the cladding. At a higher bending radius and a higher number of cladding rings, the TM mode is more constrained by the bigger air holes to spread across the silica bridges and the fields extend into the bigger air holes, which consequently increases the TM mode loss. When the bending radius is further reduced, the TM modal field then spreads beyond the first air-hole ring with larger air holes and subsequently spreads into the silica bridges beyond the first ring, which leads to the cut-off condition. The variation of the bending loss for the H_{11}^x mode for a different number of air-hole rings, N, is shown in Fig. 7. It can be observed that, when the number of air-hole rings is increased, the loss for the H_{11}^x mode is actually higher. This arises due to the fact that, for the optimized design with a larger d_2/Λ value and a relatively lower Λ value, the H_{11}^x mode is operating very close to the cutoff. By contrast, for a given bending radius, the TE modes spread less into the cladding region as they are slightly better confined and there is a delayed cutoff compared to that for the TM modes. The resulting LR loss ratios for different numbers of rings are shown in Fig. 8 and it can be observed that each has a different critical bending radius, below which LR accelerates. It can be clearly observed that the differential loss is higher when the number of air-hole rings is increased.

It is necessary to evaluate the range of d_2/Λ for which a given PCF will have SMSP operation, with a lower TE modal loss. This analysis can be carried out by evaluating the length of PCF that is necessary to offer a larger loss to the TM mode than that of the
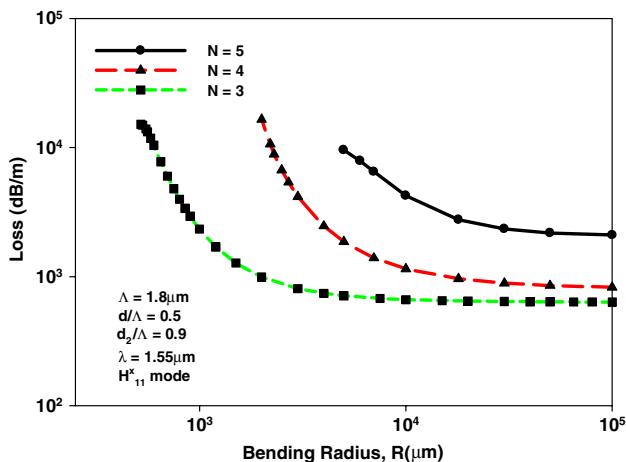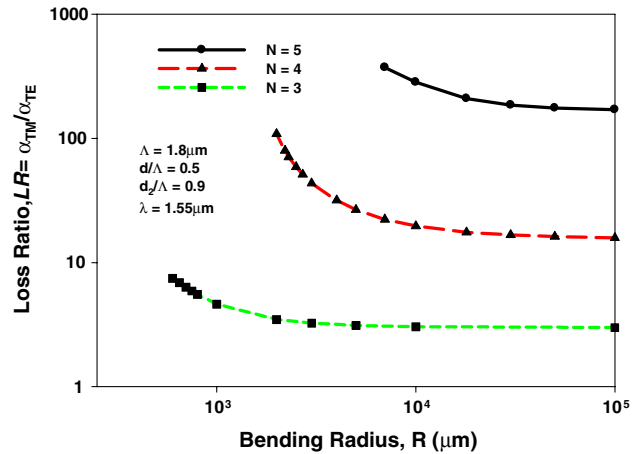

Fig. 8. (Color online) Variation of the LRs with the bending radius for different N values.

TE mode (say, by an amount of 20 dB—or any other ratio can be defined). This length of PCF, $L_{20\,dB}$, to achieve 20 dB differential loss can be defined as

$$L_{20\,dB} = \frac{20\,dB}{\alpha_{TM} - \alpha_{TE}}, \qquad (4)$$

where α_{TE} and α_{TM} are loss values for the fundamental quasi-TE and quasi-TM modes given in decibels per centimeter. Figure 9 shows the variation of a PCF with a length of $L_{20\,dB}$ (in centimeters) with respect to R for different d_2/Λ values. It can be seen that the length of the PCF section that is necessary can be of the order of a fraction of a meter and with higher pitch ratio when the TM modes can be suppressed effectively. However, a PCF for a specific application should be determined based on the combined factor of the $L_{20\,dB}$ and the total TE modal loss. From Fig. 9, it can be seen that the value of the length, $L_{20\,dB}$, can be varied over a wide range by varying the number of rings and bending radius. As an example, when $N = 5$ and R is 0.5 cm, the required PCF length to achieve the 20 dB differential loss is only 0.2 cm. However, when the bending radius is increased to 1.0 cm,
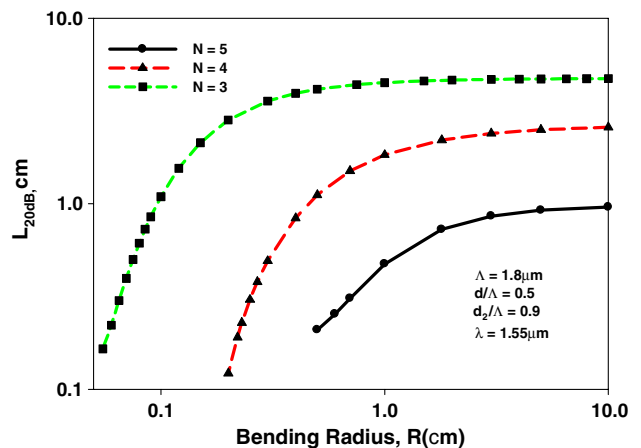

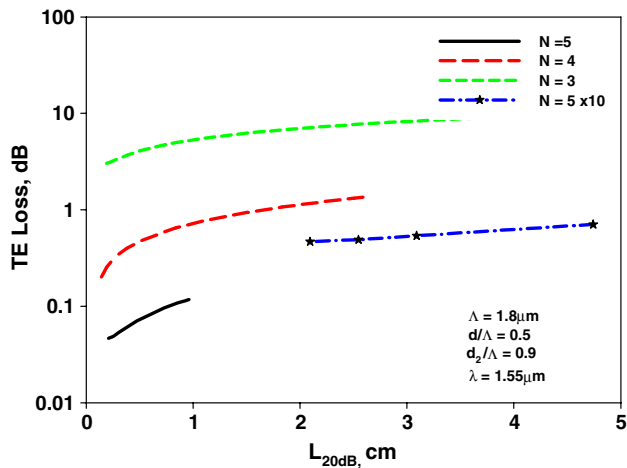Fig. 7. (Color online) Variation of LR with the bending radius for different number of rings, N.

Fig. 9. (Color online) Variation of $L_{20\,dB}$ length with the bending radius for different N values.

Fig. 10. (Color online) Variation of $L_{20\,dB}$ length with respect to the TE loss for different N values.

Fig. 11. (Color online) Variation of the loss with the bending radius for two different asymmetry orientations.

which would be easier, depending on the stiffness of the PCF, the length required would be increased to 0.4 cm, which would also be easier to handle.

For these designs, the length and corresponding total TE loss values are shown in Fig. 10 to achieve a 20 dB differential loss. It can be observed that total TE loss values could be less than 1 dB and the length of the PCF section could be below 5 cm. For the examples given earlier, with $N = 5$ and $R = 1$ cm, the required length was 0.4 cm and its corresponding total TE loss is only 0.07 dB. The length may be too short to handle it conveniently, but it should be noted that, if the length is increased by 10 times to 4 cm, which would allow it to be more easily handled, in this case the total TE loss would increase to 0.7 dB. This is still a low value and the differential loss would be 200 dB, a significantly improved value. Similarly, for $N = 5$ and $R = 0.5$ cm, if the length is increased to 2 cm, the differential loss would be 200 dB with the total TE loss only 0.5 dB. These TE loss values for a 200 dB differential loss are shown separately by a chained line with stars. Similarly other fabrication parameters, such as the pitch length, the air-hole-to-pitch ratio, d/Λ, and the asymmetry (via the d_2 value) can be adjusted to obtain a suitable design for a specific application.

The bending loss depends not only on the polarization states, as shown above, but also on the hole orientation and the bending plane. When the hole orientation is rotated by 90° (and the bending plane remains the same), modal properties and the bending loss value change. Variation of the bending loss with the bending radius for both polarization states and for both hole orientations are shown in Fig. 11. It should be noted that, in the original hole orientation [4,7], the effective height of the waveguide is smaller that its effective width. The resulting waveguide asymmetry gives the modal birefringence and the differential LR. For this particular orientation, the effective index of the H_{11}^x mode is lower and its bending loss is higher compared to the H_{11}^y mode. On the other hand, when the orientation of the larger four
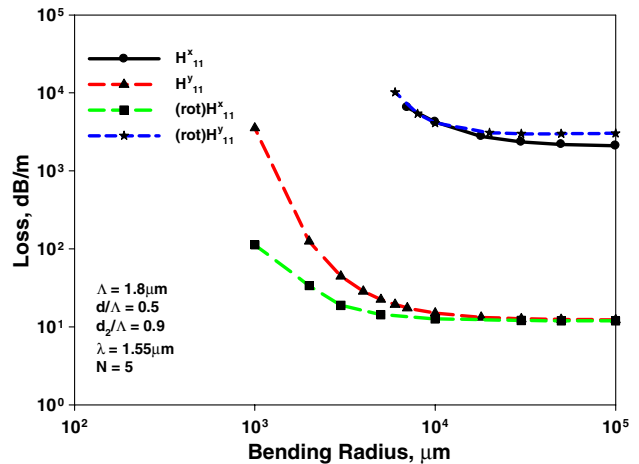
air holes is rotated by 90°, its effective height becomes smaller than its effective width. It can be observed that the bending loss of the H_{11}^y mode in the original orientation is similar to the bending loss of the H_{11}^x mode in the rotated structure, and vice versa. However, this nearly reverses the modal properties, as the H_{11}^x mode of the original orientation behaves similar to the H_{11}^y mode in the rotated structure. However, as in the bent PCF, due to the lack of symmetry along the vertical axis, the bending losses for the H_{11}^x and H_{11}^y modes are slightly different, which is clearly shown in Fig. 11.

Modal confinement and bending loss also depend on the operating wavelength. Variation of the bending loss for the quasi-TE (H_{11}^y) and quasi-TM (H_{11}^x) modes for both the original orientation and 90° rotated structures are shown in Fig. 12. In this case, the structural parameters are taken as $\Lambda = 1.8\,\mu m$, $d/\Lambda = 0.5$, $d_2/\Lambda = 0.9$, $N = 5$, and $R = 1$ cm. It can be observed that, as the operating wavelength is increased, the bending loss is increased as its modal confinement also reduces and the modal field spreads more into the cladding area. It has already
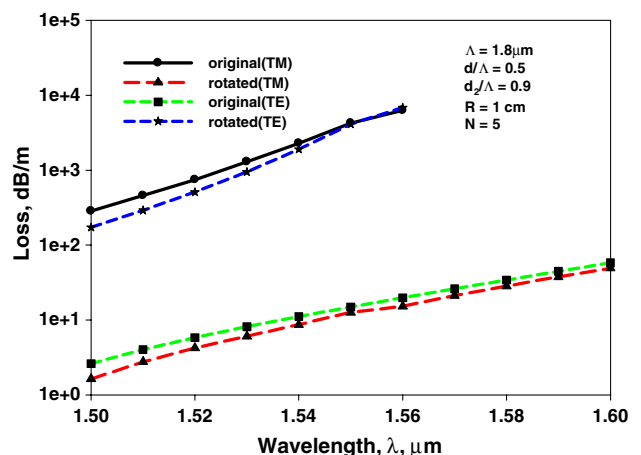

Fig. 12. (Color online) Variation of loss with the operating wavelength for two different asymmetry orientations.

been mentioned that, when the structural asymmetry is rotated by 90°, quasi-TE modes would be comparable to quasi-TM modes of the rotated structure, and vice versa.

3. Conclusion

The design of a SMSP PCF is reported here, developed by exploiting the differential bending loss and then analyzed through the use of a rigorous full-vectorial FEM. In this study, initially, the bending of the PCF has been assumed to be in the X–Y plane. This work has shown that, for this asymmetry arrangement, the TM modal loss is higher than that of the TE mode. However, the differential LR increases with any excessive bending beyond a critical value of the bending radius. Such a critical bending radius can be tuned with a suitable adjustment of the value of d_2/Λ. The LR increases with the number of air-hole rings, N, in the PCF cladding. These results can be used to assist in designing the single-polarization condition in a bent PCF. All these PCFs are also single-mode guide when operated closer to their cutoff conditions. Furthermore, the effects of structural asymmetry have also been carried out to evaluate the effect on the SMSP of a PCF due to bending for different air-hole orientations. Variations of the bending loss for the TE and TM modes with the different operating wavelengths are also presented.

Such a PCF, which only guides one polarization state, can be used for various linear, nonlinear, and sensing applications. It is also shown here that the bending losses of H_{11}^x and H_{11}^y depend on the pitch, Λ, the asymmetry via the value of d_2/Λ, the number of rings, N, the operating wavelength, and the bending radius and, so, the differential loss will depend on the fabrication tolerances relating to the parameters Λ, d, and d_2. However, since the differential loss also depends on the bending radius, it is expected that, by adjusting the bending radius, the effect of the fabrication tolerances may also be compensated for a wide range of applications.

References

1. P. St. J. Russell, "Photonic-crystal fibers," J. Lightwave Technol. **24**, 4729–4747 (2006).
2. N. A. Mortensen, "Effective area of photonic crystal fibers," Opt. Express **10**, 341–348 (2002).
3. B. T. Kuhlmey, R. C. McPhedran, and C. M. de Sterke, "Modal cutoff in microstructured optical fibers," Opt. Lett. **27**, 1684–1686 (2002).
4. N. Kejalakshmy, B. M. A. Rahman, A. Agrawal, T. Wongcharoen, and K. T. V. Grattan, "Characterization of single-polarization single-mode photonic crystal fiber using full-vectorial finite element method," Appl. Phys. B **93**, 223–230 (2008).
5. B. M. A. Rahman and J. B. Davies, "Finite-element solution of integrated optical waveguide," J. Lightwave Technol. **LT-2**, 682–688 (1984).
6. K. Saitoh and M. Koshiba, "Numerical modelling of photonic crystal fiber," J. Lightwave Technol. **23**, 3580–3590 (2005).
7. B. M. A. Rahman, A. K. M. S. Kabir, M. Rajarajan, K. T. V. Grattan, and V. Rakocevic, "Birefringence study of photonic crystal fibers by using the full-vectorial finite element method," Appl. Phys. B **84**, 75–82 (2006).
8. B. M. A. Rahman, N. Kejalakshmy, M. Uthman, A. Agrawal, T. Wongcharoen, and K. T. V. Grattan, "Mode degeneration in bent photonic crystal fiber study by using the finite element method," Appl. Opt. **48**, G131–G138 (2009).
9. M. Heiblum and J. H. Harris, "Analysis of curved optical waveguides by conformal transformation," IEEE J. Quantum Electron. **11**, 75–83 (1975).